Microchannel Flow with Patchwise and Periodic Surface Heterogeneity

David Erickson and Dongqing Li*

Department of Mechanical and Industrial Engineering, University of Toronto, 5 King's College Road, Toronto, Ontario, Canada, M5S 3G8

Received May 13, 2002. In Final Form: August 29, 2002

Surface heterogeneity is present in a variety of electrokinetic transport phenomena. It is desirable to understand the synergetic effects of the electrical double layer field and the surface heterogeneity on electrokinetic flow in microchannels. In this paper, a 3D, finite element based, numerical model for pressure-driven flow through microchannels with an arbitrary but periodic patchwise heterogeneous surface pattern has been developed. The model is based on a simultaneous solution to the Nernst−Planck, Poisson, and Navier−Stokes equations to determine the local ionic concentration, the double layer distribution, and the flow field. The presence of a heterogeneous patch is shown to induce flow in all three coordinate directions, including a circulation pattern perpendicular to the main flow axis. The strength of this circulation region is found to be proportional to Reynolds number and double layer thickness. While at low Reynolds number (i.e., Re < 1) the double layer distribution is diffusion dominated, significant convective effects are observed at higher Reynolds number leading to a deviation from the classical Poisson−Boltzmann distribution. The combined effect of the 3D flow field and disturbed double layer region on measurable quantities such as the streaming potential is discussed.

I. Introduction

Transport over heterogeneous surfaces arises in a variety of electrokinetic characterization and microfluidics-based applications. In a number of studies, the streaming potential technique has been used to monitor the dynamic or static adsorption of proteins,[1−4] surface active substances,[5] and other colloidal and nanosized particles[6,7] onto a variety of surfaces. In this technique, the surface's electrokinetic properties are altered by introducing a heterogeneous region, for example due to protein adsorption, which has a different ζ-potential than the original surface. The introduction of this heterogeneous region induces a change in the surface's average ζ-potential, which is monitored via a streaming potential measurement and related back to the degree of surface coverage.

Microfluidics-based biosensors[8−10] often involve selective capture or adhesion of a particular organism (for example *Escherichia coli*[8]) from the solution medium onto a heterogeneous probe. The presence of the organism can then be externally detected via some fluorescence or chemiluminesence method. These patches are typically arranged in a periodic fashion and in general do not necessarily have the same electrokinetic properties of the homogeneous sensing platform. In a dynamically transported medium, the capture of these particles can be sensitive to the velocity gradients near the surface, with higher velocities inducing greater shear forces tending to inhibit adhesion. Other examples of microfluidics-based applications involving surface heterogeneity include a recent study where the ability of oppositely charged patches to enhance species mixing under electroosmotic flow was demonstrated.[11] Other researchers[12−14] have investigated the use of heterogeneous capillaries, modified either chemically or through the use of radial electric fields, in capillary electrophoresis, while still others have investigated artificial manipulation of the surface ζ-potential for a number of on-chip applications.[15−16]

A variety of analytical and numerical models have been proposed recently to investigate electrokinetic effects over heterogeneous surfaces. Adamczyk et al.[7,17] proposed an approximate analytical model for spherical particles adsorbed onto a flat surface. Changes in the measured streaming potential were attributed to damping of the local fluid velocity in the region of the particle and additional charge transport from the particle surface. Hayes et al.[6,18] also presented another approximate analytical model for adsorbed particles; however, their model was based on an assumed shift in the shear plane due to particle adsorption. A few techniques for modeling electroosmotic flow over heterogeneous surfaces such as

* To whom correspondence should be addressed. E-mail: dli@mie.utoronto.ca. Fax: (416) 978-7753.

(1) Norde, W.; Rouwendal, E. *J. Colloid Interface Sci.* **1990**, *139*, 169−176.
(2) Elgersma, A. V.; Zsom, R. L. J.; Lyklema, J.; Norde, W. *Colloids Surf.* **1992**, *65*, 17−28.
(3) Zembala, M.; Déjardin, P. *Colloids Surf., B* **1994**, *3*, 119−129.
(4) Werner, C.; Jacobasch, H. J. *Macromol. Symp.* **1996**, *103*, 43−54.
(5) Fuerstenau, D. W. *J. Phys. Chem.* **1956**, *60*, 981.
(6) Hayes, R.; Böhmer, M.; Fokkink, L. *Langmuir* **1999**, *15*, 2865−2870.
(7) Zembala, M.; Adamczyk, Z. *Langmuir* **2000**, *16*, 1593−1601.
(8) Stokes, D.; Griffin, G.; Vo-Dinh, T. *Fresenius' J. Anal. Chem.* **2001**, *369*, 295−301.
(9) Cheek, B.; Steel, A.; Torres, M.; Yu, Y.-Y.; Yang, H. *Anal. Chem.* **2001**, *73*, 5777−5783.
(10) Dodge, A.; Fluri, K.; Verpoorte, E.; de Roojj, N. *Anal. Chem.* **2001**, *73*, 3400−3409.
(11) Erickson, D.; Li, D. *Langmuir* **2002**, *18*, 1883−1892.
(12) Herr, A.; Molho, J.; Santiago, J.; Mungal, M.; Kenny, T. *Anal. Chem.* **2000**, *72*, 1053−1057.
(13) Keely, C.; van de Goor, T.; McManigill, D. *Anal. Chem.* **1994**, *66*, 4236−4242.
(14) Wu, C.-T.; Huang, T.-L.; Lee, C.; Miller, C. *Anal. Chem.* **1993**, *65*, 568−571.
(15) Towns, J. K.; Regnier, F. E. *Anal. Chem.* **1992**, *64*, 2473.
(16) Nashbesh, W.; El Rassi, Z. *J. High Resolut. Chromatogr.* **1992**, *15*, 289−292.
(17) Adamczyk, Z.; Warszynzki, P.; Zembala, M. *Bull. Pol. Acad. Sci., Chem.* **1999**, *47*, 239−258.
(18) Hayes, R. *Colloids Surf., A* **1999**, *146*, 89−94.

10.1021/la025942r CCC: $22.00
Published on Web 10/16/2002

the methods of Ajdari,[19,20] Stroock et al.,[21] and Erickson and Li[11] have also been proposed. Cohen and Radke[22] presented a 2D numerical model and a perturbation technique for modeling pressure-driven flow over a flat heterogeneous region perpendicular to the flow axis. In an earlier paper,[23] we also presented a 2D numerical model for flow over a heterogeneous strip, parallel with the flow axis. With the exception of the Cohen and Radke paper,[22] all of the above studies assume a Poisson−Boltzmann double layer field. To our knowledge, however, there has not yet been an investigation into the full 3D flow structure caused by the presence of periodic patchwise surface heterogeneity and the resulting disturbance of the double layer field.

The purpose of this paper is to investigate the 3D flow structure associated with pressure-driven flow through microchannels with an arbitrary but periodic patchwise heterogeneous surface pattern. A numerical model based on a simultaneous solution, via the finite element method, to the Nernst−Planck, Poisson, and Navier−Stokes equations to determine the local ionic concentration, the double layer distribution, and the overall flow field is developed. Details of the numerical procedure are presented as well as a variety of results showing the influence of the heterogeneous patches on the flow field, electrical double layer distribution, and measured streaming potential. In addition, quantitative limits on when the Poisson−Boltzmann double layer assumption can be applied are proposed.

II. Theory and Numerical Method

In this study, we consider the two general periodically repeating surface patterns, as shown in Figure 1, which we refer to as the close-packed pattern (Figure 1A) and the loose-packed pattern (Figure 1B). In each case, the smallest periodic cell for the pattern is also shown. Although the close-packed pattern always has a percent heterogeneous coverage of 50%, the quantity can be adjusted for the loose-packed pattern by changing the size and spacing of the patches.

II.A. Model Equations. To model the situation of interest, we consider the pressure-driven flow through a parallel plate microchannel, where both the upper and lower surfaces exhibit one of the heterogeneous surface patterns discussed above. Since the pattern is repeating, the computational domain is reduced to that over a single periodic cell, similar to those shown in Figure 1. To further minimize the size of the solution domain, we assume that the heterogeneous surface pattern is symmetric about the channel mid-plane. The result is the 3D computational domain shown in Figure 2A. Generally, surfaces 3, 5, and 6 (as are labeled in Figure 2B and as will be referred to symbolically by Γ in the following discussion) represent symmetry boundaries while surfaces 2 and 4 are periodic boundaries of the computational domain. Further details regarding periodicity as related to this study are provided throughout this section; for a general discussion, the reader is referred to a paper by Patankar et al.[24]

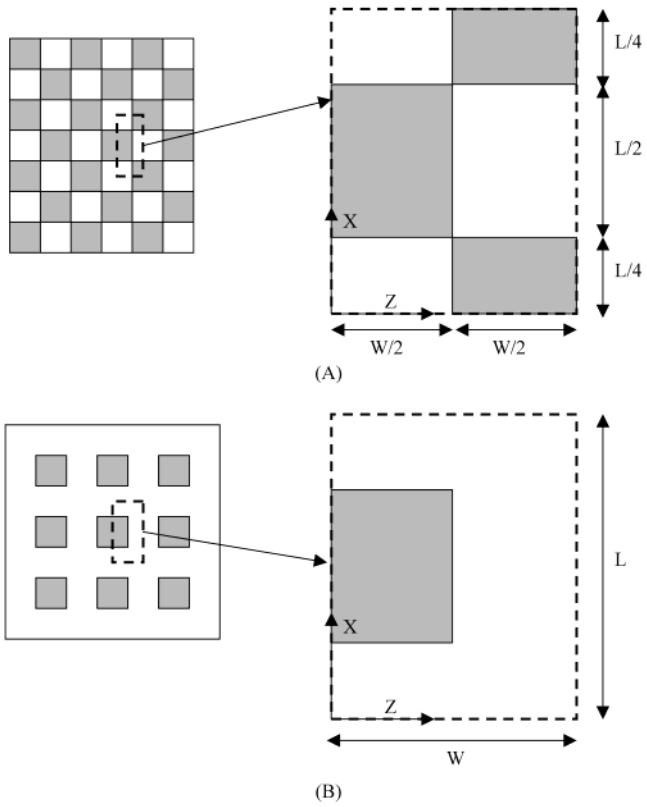

Figure 1. Simulated surface heterogeneity patterns: (A) close-packed pattern and (B) loose-packed pattern. Dark regions represent the heterogeneous patches on the surface. The dashed line represents the computational domain.

As was discussed above, to model the electrokinetic flow through this periodic unit, we require a description of the ionic species distribution, the double layer potential, the flow field, and the induced streaming potential. To begin, the divergence of the ion species flux, often referred to as the Nernst−Planck conservation equations,[25−26] is used to describe the positive and negative ion densities (given below in nondimensional form),

$$\tilde{\nabla}\cdot(-\tilde{\nabla}N^{+} - N^{+}\tilde{\nabla}\Phi + \mathrm{Pe}^{+}N^{+}V) = 0 \qquad (1a)$$

$$\tilde{\nabla}\cdot(-\tilde{\nabla}N^{-} + N^{-}\tilde{\nabla}\Phi + \mathrm{Pe}^{-}N^{-}V) = 0 \qquad (1b)$$

where N^{+} and N^{-} are the nondimensional positive and negative species concentrations ($N^{+} = n^{+}/n_0$, $N^{-} = n^{-}/n_0$ where n_0 is the bulk ionic concentration), Φ is the nondimensional electric field strength ($\Phi = e\phi/k_bT$ where e is the elemental charge, k_b is the Boltzmann constant, and T is the temperature in Kelvin), V is the nondimensional velocity ($V = v/v_0$ where v_0 is a reference velocity based on the Reynolds number), and the $\sim$ sign signifies that the gradient operator has been nondimensionalized with respect to the channel half-height (l_y in Figure 2). The two species Peclet are given by $\mathrm{Pe}^{+} = v_0 l_y/D^{+}$ and $\mathrm{Pe}^{-} = v_0 l_y/D^{-}$ where D^{+} and D^{-} are the diffusion coefficients for the positive and negative species, respectively. For completeness, it is important to note that in the derivation of the above equations we have assumed that the ionic species are monovalent.

(19) Ajdari, A. *Phys. Rev. Lett.* **1995**, *75* (4), 755−758.
(20) Ajdari, A. *Phys. Rev. E* **1996**, *53* (5), 4996−5005.
(21) Stroock, A. D.; Weck, M.; Chiu, D. T.; Huck, W. T. S.; Kenis, P. J. A.; Ismagilov, R. F.; Whitesides, G. M. *Phys. Rev. Lett.* **2000**, *84* (15), 3314−3317. Also see: Stroock, A. D.; Weck, M.; Chiu, D. T.; Huck, W. T. S.; Kenis, P. J. A.; Ismagilov, R. F.; Whitesides, G. M. *Phys. Rev. Lett.* **2001**, *86* (26), 6050.
(22) Cohen, R.; Radke, C. *J. Colloid Interface Sci.* **1991**, *141*, 338−347.
(23) Erickson, D.; Li, D. *J. Colloid Interface Sci.* **2001**, *237*, 283−289.
(24) Patankar, S.; Liu, C.; Sparrow, E. *J. Heat Transfer* **1977**, *99* (2), 180−186.
(25) Lyklema, J. *Fundamentals of Interface and Colloid Science, Volume 1*: *Fundamentals*; Academic Press: San Diego, 1991.
(26) Lyklema, J. *Fundamentals of Interface and Colloid Science, Volume 2*: *Solid−Liquid Interfaces*; Academic Press: San Diego, 1995.

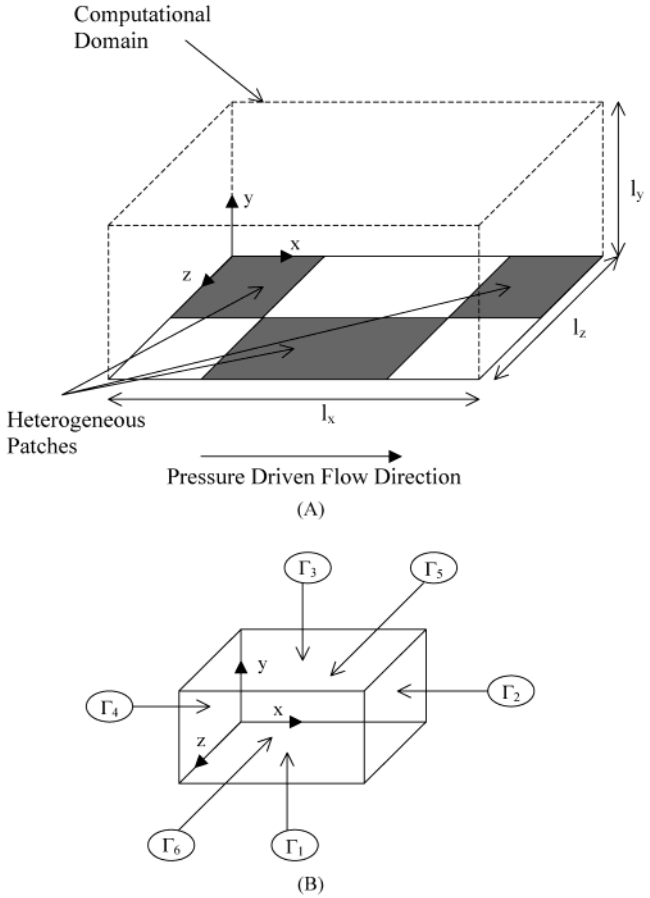

Figure 2. (A) Computational domain for the 3D spatially periodic cell, showing the heterogeneous surface pattern. (B) Labels for surfaces. Γ_1 represents the heterogeneous surface plane; Γ_3, Γ_5, and Γ_6 are symmetry surfaces; Γ_2 and Γ_4 are periodic surfaces.

Along the wall (surface 1 in Figure 2B) and symmetry boundaries of the computational domain, zero flux boundary conditions are applied,

$$-\frac{\partial N^+}{\partial Y} - N^+\frac{\partial \Phi}{\partial Y} = 0 \qquad \text{on } \Gamma_1, \Gamma_3 \tag{1c}$$

$$-\frac{\partial N^-}{\partial Y} + N^-\frac{\partial \Phi}{\partial Y} = 0 \qquad \text{on } \Gamma_1, \Gamma_3 \tag{1d}$$

$$-\frac{\partial N^+}{\partial Z} - N^+\frac{\partial \Phi}{\partial Z} = 0 \qquad \text{on } \Gamma_5, \Gamma_6 \tag{1e}$$

$$-\frac{\partial N^+}{\partial Z} + N^-\frac{\partial \Phi}{\partial Z} = 0 \qquad \text{on } \Gamma_5, \Gamma_6 \tag{1f}$$

where X, Y, and Z are the nondimensional coordinate directions ($X = x/l_y$, $Y = y/l_y$, and $Z = z/l_y$). Note that in the above boundary conditions the velocity flux components need not be considered as V perpendicular to these surfaces must be zero, as will be discussed later. Periodic conditions are applied along faces 2 and 4 as below,

$$N_2^+ = N_4^+ \qquad \text{on } \Gamma_2, \Gamma_4 \tag{1g}$$

$$N_2^- = N_4^- \qquad \text{on } \Gamma_2, \Gamma_4 \tag{1h}$$

The velocity field is described by the Navier−Stokes equations for momentum, modified to account for the electrokinetic body force, and the continuity equation as shown below,

$$\mathrm{Re}(V\cdot\tilde{\nabla}V) = -\bar{\nabla}P + \tilde{\nabla}^2V - F(N^+ - N^-)\tilde{\nabla}\Phi \tag{2a}$$

$$\tilde{\nabla}\cdot V = 0 \tag{2b}$$

where F is a nondimensional constant ($F = n_0 l_y k_b T/\mu v_0$) which accounts for the electrokinetic body force responsible for electroosmotic and electroviscous effects, Re is the Reynolds number ($\mathrm{Re} = \rho v_0 l_y/\mu$, where ρ is the fluid density and μ is the viscosity), and P is the nondimensional pressure. As in the previous case, periodic boundary conditions are applied along Γ_2 and Γ_4 as below,

$$\begin{aligned} V_{x,2} &= V_{x,4} \\ V_{y,2} &= V_{y,4} \qquad \text{on } \Gamma_2, \Gamma_4 \\ V_{z,2} &= V_{z,4} \end{aligned} \tag{2c}$$

A no-slip condition is applied along the heterogeneous surface (the channel wall) as described by eq 2d,

$$V_x = V_y = V_z = 0 \qquad \text{on } \Gamma_1 \tag{2d}$$

Along the upper symmetry surface, we enforce a zero penetration condition for the y component of velocity and zero gradient conditions for the x and z terms respectively,

$$\frac{\partial V_x}{\partial Y} = V_y = \frac{\partial V_z}{\partial Y} = 0 \qquad \text{on } \Gamma_3 \tag{2e}$$

Similarly, a zero penetration condition for the z component of velocity is applied along Γ_5 and Γ_6 while zero gradient conditions are enforced for the x and y components,

$$\frac{\partial V_x}{\partial Z} = \frac{\partial V_y}{\partial Z} = V_z = 0 \qquad \text{on } \Gamma_5, \Gamma_6 \tag{2f}$$

The remaining quantity that must be described is the nondimensional electric field strength. We begin by separating the total electric field strength Φ into two components as has been done by a number of authors; for examples, see Cohen and Radke[22] and Masyliyah:[27]

$$\Phi(X,Y,Z) = \Psi(X,Y,Z) + \mathrm{E}(X) \tag{3}$$

where the first component, $\Psi(X,Y)$, describes the electrical double layer field and the second component, $\mathrm{E}(X)$, describes the induced electric field resulting from the streaming potential. In general, the double layer component of Φ is described by a Poisson distribution as shown below,

$$\bar{\nabla}^2\Psi + K^2(N^+ - N^-) = 0 \tag{4a}$$

where K is the nondimensional double layer thickness ($K = l_y^2 n_0 e^2/k_b T\epsilon_w$). Two boundary conditions commonly applied along the solid surface for the above equation are either an enforced potential gradient proportional to the surface charge density or a fixed potential condition equivalent to the surface ζ-potential. In this study, we opt for the latter given by

$$\Psi = \mathrm{Z}(x,z) \qquad \text{on } \Gamma_1 \tag{4b}$$

where Z is the nondimensional ζ-potential ($\mathrm{Z} = e\zeta/k_b T$). Along the upper and side boundaries of the computational

(27) Masliyah, J. *J. Colloid Interface Sci.* **1994**, *166*, 383−393.

domain, symmetry conditions (eq 4c and eq 4d) are applied, and periodic conditions (eq 4e) are applied at the inlet and outlet, as below,

$$\frac{\partial \Psi}{\partial Y} = 0 \qquad \text{on } \Gamma_3 \tag{4c}$$

$$\frac{\partial \Psi}{\partial Z} = 0 \qquad \text{on } \Gamma_5, \Gamma_6 \tag{4d}$$

$$\Psi_2 = \Psi_4 \qquad \text{on } \Gamma_2, \Gamma_4 \tag{4e}$$

Extending into three dimensions the technique used by Cohen and Radke,[22] the component E is evaluated from the condition that the net current flux is zero for constant x, described in general by eq 5a,

$$J(X) = \int_0^{Z_{max}} \int_0^{Y_{max}} [J^+(X,Y,Z) - J^-(X,Y,Z)] \cdot n_x \, dY \, dZ = 0 \tag{5a}$$

where n_x in the above is a normal vector in the x direction and J^+ and J^- are the nondimensional positive and negative current densities. Assuming monovalent ions for both positive and negative species (as was discussed earlier) and using the ionic species flux terms from eq 1a and eq 1b, condition 5a reduces to the following,

$$\int_0^{Z_{max}} \int_0^{Y_{max}} \left(-\left[\frac{\partial N^+}{\partial X} - \frac{Br^+}{Br^-} \frac{\partial N^-}{\partial X} \right] - \left[N^+ + \frac{Br^+}{Br^-} N^- \right] \frac{\partial (\Psi + E)}{\partial X} + [\mathrm{Pe}^+ (N^+ - N^-) V_x] \right) dY \, dZ = 0 \tag{5b}$$

which is a balance between the conduction (term 2) and convection (term 3) currents with an additional term to account for any induced current due to concentration gradients. Solving eq 5b for the streaming potential gradient yields the final form of condition 5a given below,

$$\frac{\partial E}{\partial X} = \frac{\int_0^{Z_{max}} \int_0^{Y_{max}} \left(-\left[\frac{\partial N^+}{\partial X} - \frac{Br^+}{Br^-} \frac{\partial N^-}{\partial X} \right] - \left[N^+ + \frac{Br^+}{Br^-} N^- \right] \frac{\partial \Psi}{\partial X} + [\mathrm{Pe}^+ (N^+ - N^-) V_x] \right) dY \, dZ}{\int_0^{Z_{max}} \int_0^{Y_{max}} \left(N^+ + \frac{Br^+}{Br^-} N^- \right) dY \, dZ} \tag{5c}$$

II.B. Numerical Method and Verification. Before continuing, a detailed discussion regarding the numerical technique used to solve the above set of equations is warranted. In general, the above system of equations were solved with the finite element method[28] using an in-house written code. To begin, the computational domain was discretized using 27-noded 3D elements, which were refined within the double layer region near the surface and further refined in locations where discontinuities in the surface ζ-potential were present (i.e., the boundaries between patches). Triquadratic basis functions were used for all the unknowns N^+, N^-, V_x, V_y, V_z, and Ψ. In general, the use of these higher order elements and basis functions (as opposed to 8-noded trilinear elements) was found to be optimal as they could better approximate the sharp gradients in velocity, species concentration, and electric potential within the double layer region. Some experimentation with exponential basis functions was performed; however, due to difficulties with convergence of the solution this approach was abandoned. In all cases, periodic conditions were imposed using the technique described by Sáez and Carbonell.[29]

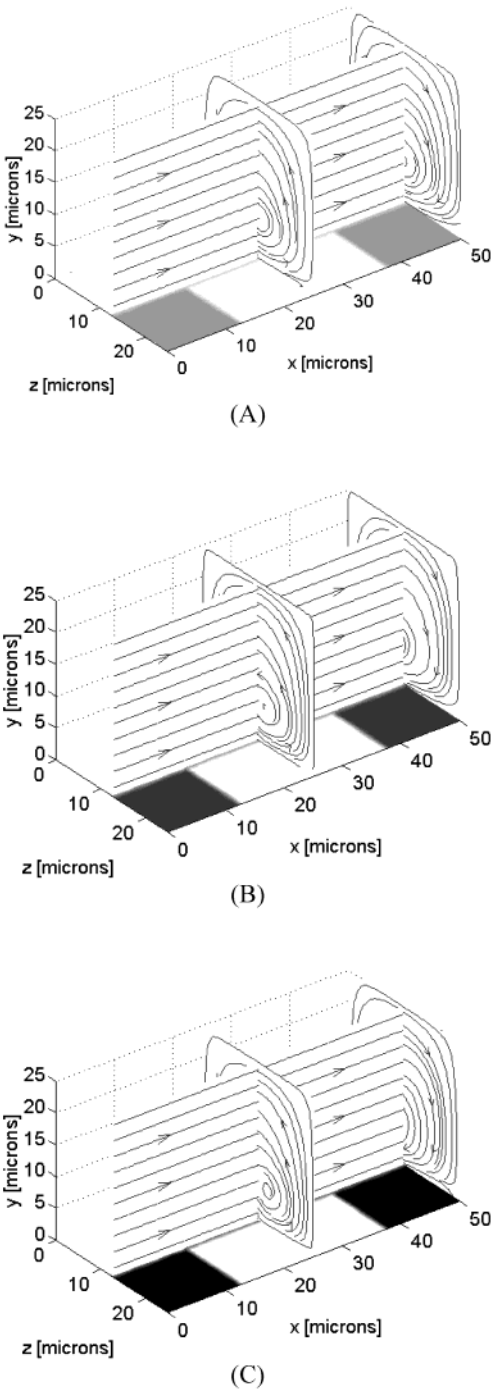

Figure 3. Influence of heterogeneous patches on flow field streamlines for the close-packed pattern. Homogeneous ζ-potential = −60 mV (white region); heterogeneous patches (dark patches) have ζ-potentials of (A) −40 mV, (B) −20 mV, and (C) 0 mV. In all cases, Re = 1 and $n_0 = 1 \times 10^{-5}$ M KCl.

After the computational mesh was formed and the elemental matrix integrations were performed,[28] an initial parabolic velocity profile was assumed and the streaming potential gradient was set to zero everywhere. The solution procedure began with a semi-implicit, nonlinear technique

(28) Heinrich, J. C.; Pepper, D. W. *Intermediate Finite Element Method*; Taylor & Francis: Philadelphia, 1999.

(29) Sáez, A.; Carbonell, R. *Int. J. Numer. Methods Fluids* **1985**, *5*, 601−614.

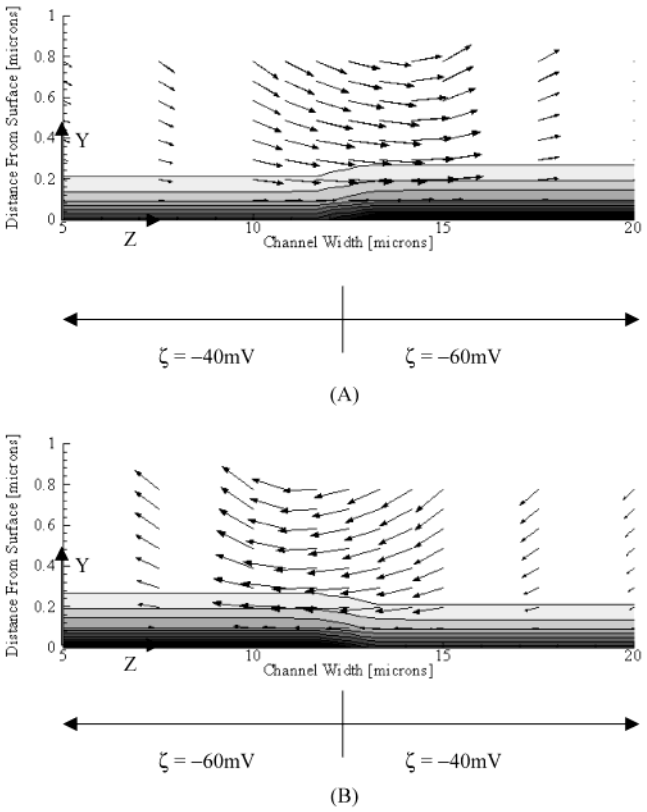

Figure 4. Velocity vectors and electrostatic potential contours in the double layer region at (A) $x = 25\ \mu$m (mid-plane) and (B) $x = 50\ \mu$m (end-plane) for the close-packed heterogeneous surface pattern. In each case, Re = 1, $n_0 = 1 \times 10^{-5}$ M KCl, and the ζ-potentials of the homogeneous region and heterogeneous patch are $\zeta_0 = -60$ mV and $\zeta_p = -40$ mV, respectively.

in which the ionic species concentrations and the double layer potential equations, eqs 1a, 1b, and 4a, were solved for simultaneously. In general, it was found that the convergence could be achieved only when the double layer potential, Ψ, in the nonlinear terms of eq 1a and eq 1b was fully implicit to the solution and the N^+ and N^- terms were explicit. An iterative procedure was then initiated, each time updating the explicit variables, until convergence on all three variables was achieved. In general, it was found that a direct solver was required as the resulting matrix was neither symmetric nor well conditioned.

Once a solution for N^+, N^-, and Ψ was obtained, the forcing term in the Navier−Stokes equations could be evaluated and eq 2a and eq 2b were solved concurrently using a penalty method[28] which eliminated the pressure term from the formulation. While this reduced the number of equations that had to be solved, the resulting poorly conditioned matrix dictated the use of a direct solver over a potentially faster iterative solver. To facilitate convergence, the static pressure (evaluated when $V_x, V_y, V_z = 0$) induced by the Y direction electric field gradients in the double layer region was subtracted from the result. Since the inlet velocity profile was not known ahead of time, the pressure drop across the computational domain was introduced via a pressure body force as was suggested by Sáez and Carbonell.[29]

Once the flow solution was obtained, eq 5c was evaluated at each cross section to yield updated values of E (streaming potential) at each point in the domain. With this result and that of the double layer potential, Ψ, the Φ term in eq 3 was updated and the above process was repeated until convergence of the $\partial E/\partial X$ was achieved. Typically, a single iterative solution to the ionic species

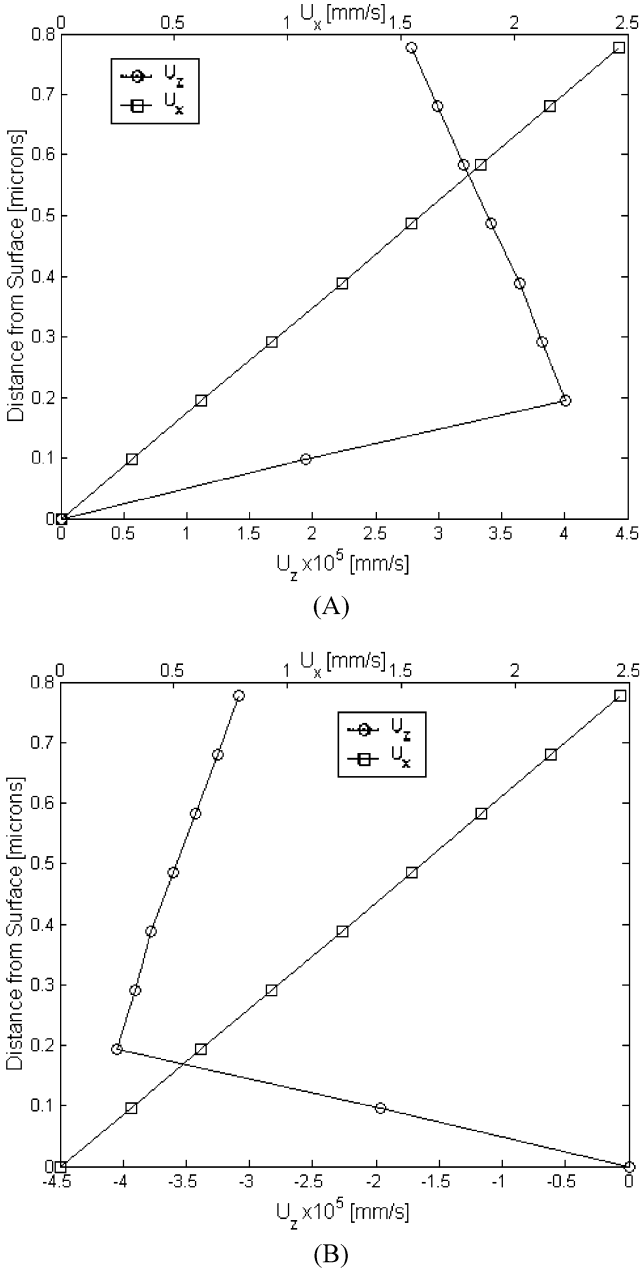

Figure 5. V_x and V_z at the midpoint ($z = 12.5\ \mu$m) of the (A) mid-plane ($x = 25\ \mu$m) and (B) end-plane ($x = 50\ \mu$m) of the close-packed heterogeneous surface pattern. In each case, Re = 1, $n_0 = 1 \times 10^{-5}$ M KCl, and the ζ-potentials of the homogeneous region and heterogeneous patch are $\zeta_0 = -60$ mV and $\zeta_p = -40$ mV, respectively.

concentrations and double layer potential system of equations required 800 s on a 2000 MHz, Pentium 4 machine with 1000 MB of memory and approximately 20 h was required to obtain final convergence of the streaming potential gradient.

Several model verification stages were undertaken in order to ensure the accuracy of the results presented here. Results from the 3D model were compared against well-known classical results for homogeneous surfaces[25,26] as well as those modified to account for electroviscous effects.[30] For heterogeneous surfaces, the model was also checked against the 2D numerical work of Cohen and Radke.[22] A mesh refinement study was also undertaken

(30) Erickson, D.; Li, D.; Werner, C. *J. Colloid Interface Sci.* **2000**, *232*, 186−197.

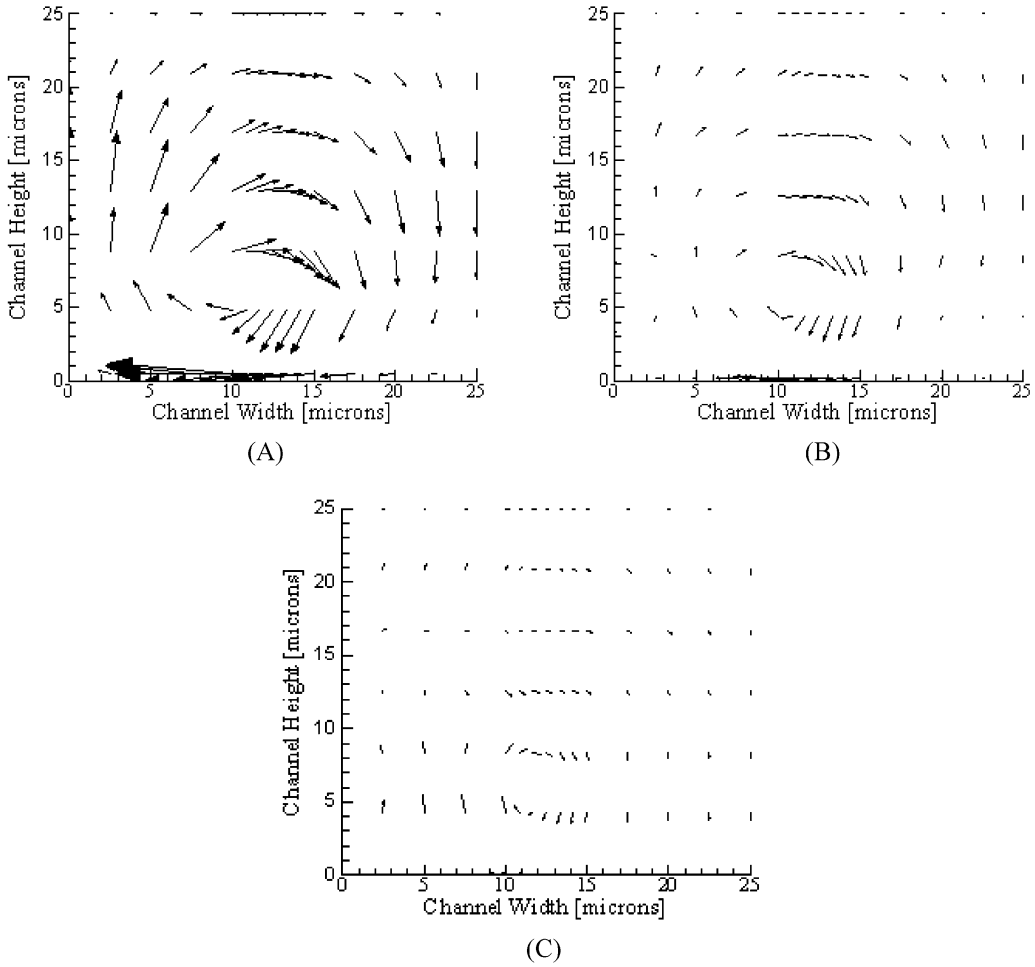

Figure 6. Velocity vectors at the mid-plane of the close-packed heterogeneous surface pattern at Re = 1 with bulk ionic concentrations of (A) $n_0 = 1 \times 10^{-5}$ M, (B) $n_0 = 1 \times 10^{-4}$ M, and (C) $n_0 = 1 \times 10^{-3}$ M. In each case, the ζ-potentials of the homogeneous region and heterogeneous patch are $\zeta_0 = -60$ mV and $\zeta_p = -20$ mV, respectively.

to ensure grid independence of the results. In addition, the numerical flow code used in this study has been checked against several classical flow test problems, such as flow over a backward step and flow in a square cavity, and has been used and experimentally verified in previous works.[31]

III. Results and Discussion

III.A. Influence of Surface Heterogeneity on the Flow Field. As mentioned earlier, the purpose of this study is to investigate the effects of surface heterogeneity on pressure-driven flow through a microchannel. First we consider the flow over a close-packed periodic surface (Figure 1A) with a periodic length $L = 50$ μm, width $W = 25$ μm, and channel height $H = 50$ μm ($H/2 = l_y$ in Figure 2). The liquid is considered as an aqueous solution of a monovalent species (physical properties of KCl from ref 32 are used here) with a bulk ionic concentration of 1×10^{-5} M. The Reynolds number Re = 1 and a homogeneous ζ-potential (i.e., the white parts of the surfaces in Figure 1 and Figure 2) of -60 mV were selected for the calculations.

Figure 3 shows the flow streamlines for different heterogeneous ζ-potentials (the dark parts of the surfaces in Figure 1 and Figure 2), -40 mV (A), -20 mV (B), and 0 mV (C). In each case, the homogeneous surface (with a ζ-potential of -60 mV) is represented by the white regions while the heterogeneous patches are shown in varying gray-scale degrees (i.e., darker for lower (i.e., less negative) ζ-potential) from A to C. As can be seen, the streamlines along the main flow axis (x-axis from Figure 2) remain relatively straight, as would be expected for typical pressure-driven flow; however, perpendicular to the main flow axis a distinct circular flow pattern can be observed. In all cases, the circulation in this plane is such that the flow near the surface is always directed from the lower ζ-potential region (in these cases the heterogeneous patch) to the higher ζ-potential region. As a result, the direction of circulation is constantly changing from clockwise to counterclockwise along the x-axis as the heterogeneous patch location switches from the right to the left side. It can also be observed that the center of circulation region tends to shift toward the high ζ-potential region as the difference in the magnitude of the homogeneous and heterogeneous ζ-potential is increased.

The observed flow circulation perpendicular to the pressure-driven flow axis is the result of an electroosmotic body force applied to the fluid continua caused by the differences in electrostatic potential between the homogeneous surface and the heterogeneous patch. Figure 4 shows the velocity vectors within the double layer region, for both the mid-plane at $x = 25$ μm (A) and the end-plane at $x = 50$ μm (B), superimposed over a contour plot of the

(31) Sinton, D.; Erickson, D.; Li, D. Submitted.
(32) Vanysek, P. Ionic Conductivity and Diffusion at Infinite Dilution. In *CRC Handbook of Chemistry and Physics*, 81st ed.; CRC Press: Boca Raton, FL, 2001.

double layer potential for the case shown in Figure 3A. The solid lines on the contour plots of this figure are equipotential lines, and darker regions represent a more negative potential (with respect to the neutral bulk solution). As can be seen in Figure 4A, a negative potential gradient exists near the transition zone between the two regions for the mid-plane. As there is an excess of positive ions in the double layer region, this potential gradient induces a body force in the positive z direction, as is described by eq 2a. The effect is similar to that observed in traditional electroosmotic flow where the excess positive charge in the double layer region is attracted to the negative electrode, inducing flow in the direction of the negative potential gradient. A similar effect can be seen in Figure 4B where now a positive potential gradient exits at the outlet plane inducing a flow in the negative z direction and resulting in the observed clockwise circulation. Simulations conducted for the loose-packed surface pattern also exhibited a similar circulation pattern; however, the magnitude tended to be significantly weaker at the inlet and exit as the ζ-potential is homogeneous along the z-axis in these regions.

In Figure 5A,B, we compare the near-surface z-directional velocity at the midpoint ($z = 12.5\ \mu$m) of the mid-plane (A) and end-plane (B) with that of the x-directional velocity, again for the case shown in Figure 3A. As can be seen, the z-directional velocity exhibits a very sharp increase near the wall, where both the excess positive ion concentration is the highest and the potential gradient is the strongest, reaches a maximum, and then begins to taper off. Note that the discontinuity in the velocity is a numerical artifact resulting from the refinement of the mesh in the double layer region and the actual flow would exhibit a smoother transition. By comparison of the relative magnitude of the two velocities, it can be seen that the maximum z-directional velocity is 4×10^{-5} mm/s versus 6×10^{-1} mm/s for the x-directional velocity at a comparable distance from the surface. This indicates that the strength of the circulation regions is significantly lower than that of the main bulk flow. Though the absolute magnitude of the velocity is relatively low, especially far away from the surface, the relatively sharp gradient within the double layer region, resulting in a relatively strong shear force, may be important to adhesion phenomena.

Since, as described above, the formation of these circulation regions is a double layer driven effect, it is of interest to investigate the influence of the double layer thickness, or alternatively the bulk ionic concentration, on the strength of the circulation. Figure 6 shows vector plots of the velocities in the end-plane of the system shown in Figure 3B for the following three ionic concentrations: (A) 1×10^{-5} M, (B) 1×10^{-4} M, and (C) 1×10^{-3} M, corresponding to the double layer thickness $1/\kappa$ ($\kappa = Kl_y$ from eq 4a) of 97, 31, and 9.7 nm, respectively. From Figure 6, it is apparent that the strength of the circulation decreases significantly with the double layer thickness. In general, over the concentration range investigated here, it was found that the magnitude of the velocity in the circulation plane was approximately proportional to the double layer thickness.

Another parameter of interest, which may affect the magnitude of the circulation velocity, is the flow Reynolds number. In Figure 7, the z-directional velocity at the midpoint ($z = 12.5\ \mu$m) of the mid-plane (A) and end-plane (B), similar to Figure 6, is presented for Reynolds number varying from Re = 0.1 to Re = 10 for the heterogeneous case shown in Figure 3A. This range of Reynolds number was selected as it is typical of those encountered in microfluidics and electrokinetic studies.

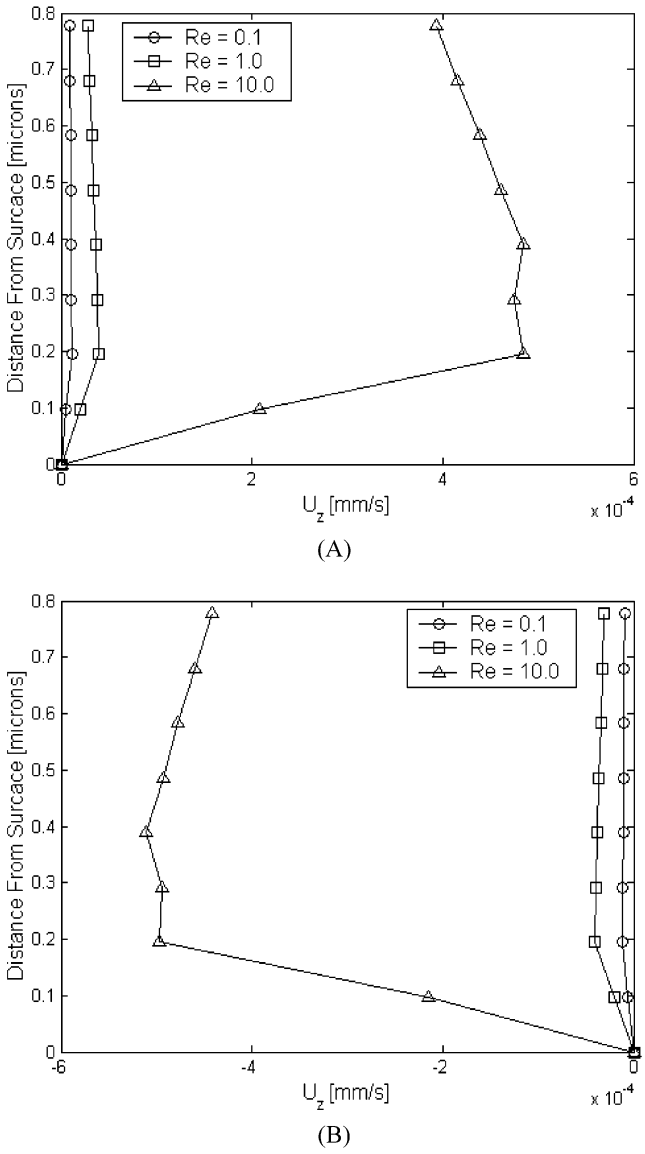

Figure 7. V_z at the midpoint ($z = 12.5\ \mu$m) of the (A) mid-plane ($x = 25\ \mu$m) and (B) end-plane ($x = 50\ \mu$m) of the close-packed heterogeneous surface pattern for various Reynolds numbers. In each case, the ζ-potentials of the homogeneous region and heterogeneous patch are $\zeta_0 = -60$ mV and $\zeta_p = -40$ mV, respectively, and the bulk ionic concentration is $n_0 = 1 \times 10^{-5}$ M.

As can be seen from these figures, the magnitude of the z component of velocity in the double layer increases significantly with Reynolds number. In general, it was found that the magnitude of the velocity within this double layer region was proportional to Reynolds number, in that the magnitude increased approximately 10-fold between Re = 0.1 and Re = 1 and similarly between Re = 1 and Re = 10.

III.B. Influence of the Induced Flow Field on the Double Layer Distribution. Figures 8 and 9 show the influence of the flow field on the double layer distribution for the Γ_5 ($z = 0\ \mu$m, Figure 8) and Γ_6 ($z = 25\ \mu$m, Figure 9) surfaces for the close-packed surface pattern at Reynolds numbers of (A) Re = 0.1, (B) Re = 1, and (C) Re = 10. In all cases, the heterogeneous ζ-potential is -40 mV and the bulk ionic concentration is 1×10^{-5} M. In both cases, it can be seen that the double layer field becomes significantly distorted at higher Reynolds numbers, when compared to the diffusion-dominated field at Re = 0.1 and

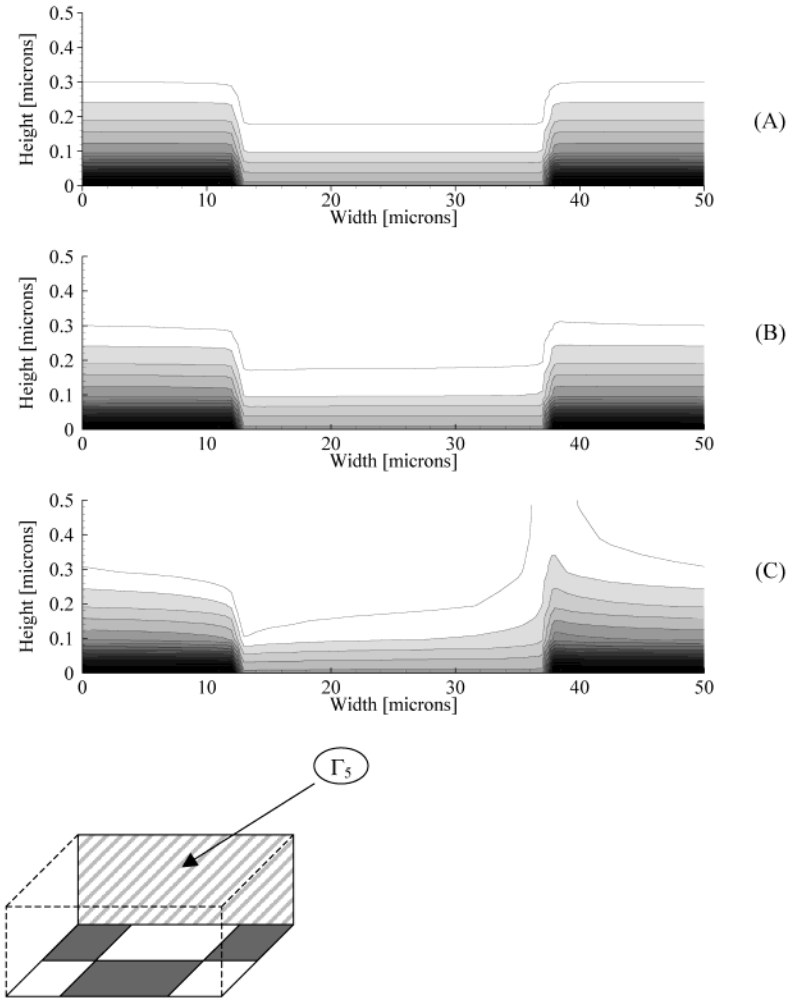

Figure 8. Electrostatic potential contours in the double layer region parallel with the flow axis on Γ_5 ($z = 0$ μm) for (A) Re = 0.1, (B) Re = 1.0, and (C) Re = 10.0 for the close-packed heterogeneous surface pattern. In each case, the ζ-potentials of the homogeneous region and heterogeneous patch are $\zeta_0 = -60$ mV and $\zeta_p = -40$ mV, respectively, and the bulk ionic concentration is $n_0 = 1 \times 10^{-5}$ M.

Re = 1. The diffusion-dominated field in these cases represents a classical Poisson−Boltzmann distribution. This distortion of the double layer field is the result of a convective effect observed by Cohen and Radke[22] in their 2D numerical work and comes about as a result of an induced *y*-directional velocity in the transition region between the two heterogeneous surfaces. This velocity perpendicular to the surface comes about as a result of the fact that the electroviscous effect is weaker over the lower ζ-potential heterogeneous patch (see ref 33 for a discussion on the electroviscous effect) and thus the velocity in the double layer region is faster in this region. To maintain continuity, then, a negative *y*-directional velocity is induced when flow is directed from a higher ζ-potential region (i.e., more negative) to a lower and a positive *y*-directional velocity is induced for the opposite case. Though Cohen and Radke[22] observed the flow field effects, a direct comparison between the disturbed and undisturbed double layer fields was not made.

The magnitude of this induced velocity is plotted in Figure 10 at the (A) high ζ-potential to low ζ-potential transition point at $x = 12.5$ μm and (B) low ζ-potential to high ζ-potential transition point at $x = 37.5$ μm. In both cases, the results are presented for the Γ_5 plane as shown in Figure 8. As can be seen, the magnitude of this velocity increases proportionally to the Reynolds number. However, this induced velocity is still significantly lower than the magnitude of the main flow velocity (see Figure 5) and thus does not significantly influence the streamlines along the flow axis shown in Figure 3. Relating Figure 10 back to the double layer distribution shown in Figure 8, it is apparent that the convective influence of the negative *y*-velocity at the first transition point led to a compression of the double layer while the positive *y*-velocity at the second transition point led to an expansion.

As alluded to earlier, in the vast majority of studies involving electrokinetic flow a Poisson−Boltzmann double layer distribution is assumed. At this point, then, we are in a position to reflect on the consequences of the results presented above with regard to these classical modeling techniques and propose some quantitative limitations on their applicability. Referring back to Figures 8 and 9 in the absence of strong convective effects, Re = 0.1 and even Re = 1.0, the double layer field reduces to a Poisson−Boltzmann distribution and it is only at Re = 10 and ionic concentration of 10^{-5} M that significant convective effects are observed. Thus we can infer that a Poisson−Boltzmann distribution is a suitable approximation so long as Re $\leq$ 1 and $n_0 \geq 10^{-5}$ M, in the case where pressure-driven flow is directed parallel with the surface plane. In more general cases, we can infer from Figure 10 that the velocity normal to the surface in the double layer must be on the order of 10^{-3} mm/s before a significant non-Poisson−Boltzmann

(33) Li, D. *Colloids Surf., A* **2001**, *195*, 35−57.

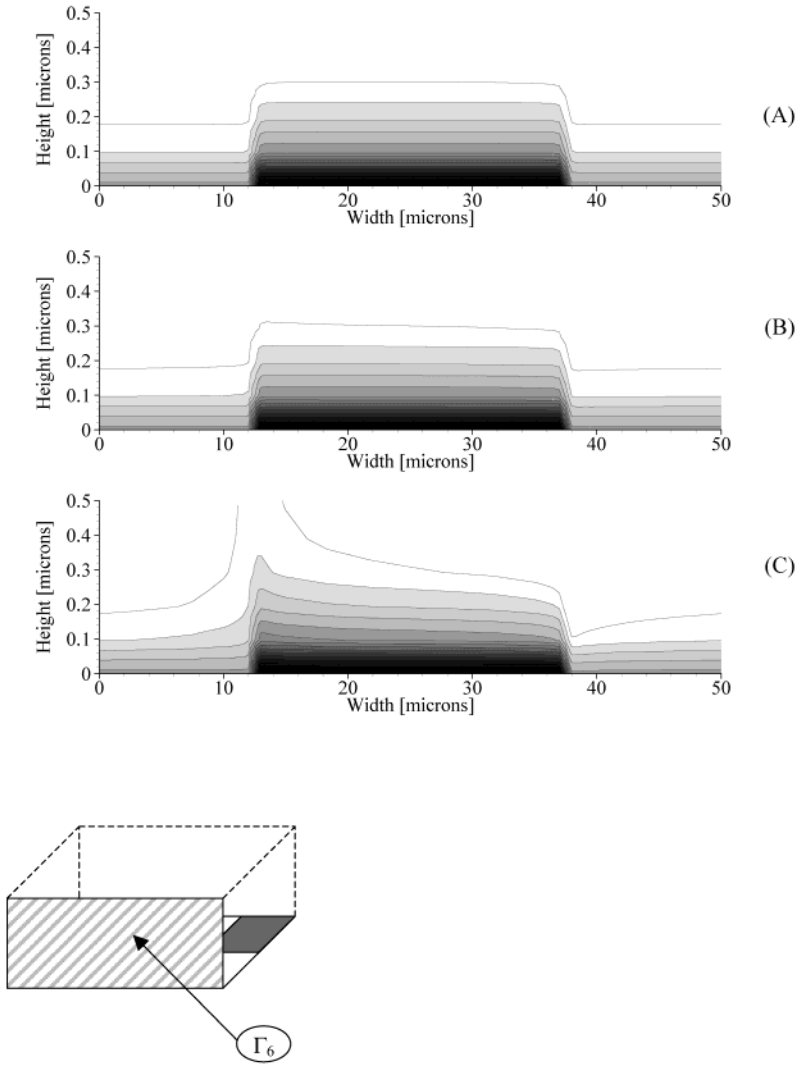

Figure 9. Electrostatic potential contours in the double layer region parallel with the flow axis on Γ_6 ($z = 25\ \mu$m) for (A) Re = 0.1, (B) Re = 1.0, and (C) Re = 10.0 for the close-packed heterogeneous surface pattern. In each case, the ζ-potentials of the homogeneous region and heterogeneous patch are $\zeta_0 = -60$ mV and $\zeta_p = -40$ mV, respectively, and the bulk ionic concentration is $n_0 = 1 \times 10^{-5}$ M.

distribution will be observed. Though in principle the mechanisms are the same, it is not clear based on the above results if these limitations are also applicable to modeling electroosmotically driven flows over heterogeneous surfaces,[11,19−21] and thus in a future work we plan to investigate this in more detail.

III.C. Special Case: Oppositely Charged Heterogeneous Patches. A special case of theoretical interest to this study occurs when the heterogeneous patches have an equal but opposite charge to that of the homogeneous surface (i.e., the surface has a ζ-potential of −60 mV while the heterogeneous patches have a ζ-potential of +60 mV). In such a case, there is an excess of positive ions over the homogeneous surface, as before, but negative ions dominate over the heterogeneous surface to balance out the positive surface charge as is shown in Figure 11. The difference in the surface potential results in an electrostatic potential gradient within the double layer region near the transition zone between the two regions similar to that shown in Figure 4B. As before, the presence of this potential gradient results in a body force on the ions in the double layer; however, in this case an opposite body force is applied to the negative ions over the positively charged patch, as shown in the detailed image in Figure 11. As a result, the net body force over the region is zero and the circulation velocity perpendicular to the main flow, as shown in Figure 3, becomes negligible.

Figure 12 shows a contour plot of the double layer potential field along the Γ_5 (A) and Γ_6 (B) planes, as defined in Figure 2, for the ζ-potential case described above using the close-packed surface pattern with a bulk ionic concentration of 1×10^{-5} M and a Reynolds number of 10. Note that in this figure the darkest region corresponds to the −60 mV surface, as before, while the lightest is the +60 mV heterogeneous patch. As can be seen, the convective influence on the double layer region is identical for both cases unlike in previous cases where an asymmetry existed depending on the direction of the streaming potential induced y-directional velocity (Figures 8 and 9). In this case, however, the net streaming potential is negligible (since the average ζ-potential is zero) and this effect is thus much smaller. The variations in the surface potential observed here are induced as a result of oppositely charged ions being transported (through both advection and diffusion) from one region to the other. In the first transition region shown in Figure 12A, for example, positive ions are being transported from the homogeneous region to the heterogeneous patch. As a result, this decreases the local net negative charge density and a disturbance of the local electric potential field is

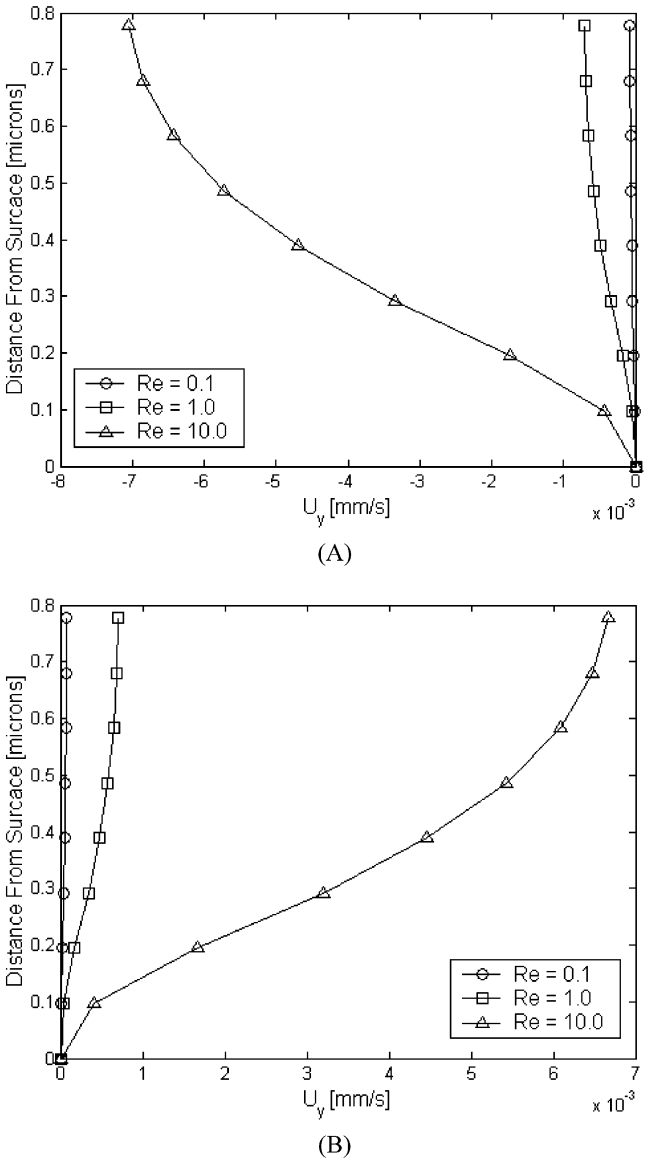

Figure 10. V_y in the double layer region at various Reynolds numbers for (A) the first ζ-potential step change, $x = 12.5\ \mu$m, and (B) the second ζ-potential step change, $x = 37.5\ \mu$m, along Γ_5 for the close-packed heterogeneous surface pattern. In each case, the ζ-potentials of the homogeneous region and heterogeneous patch are $\zeta_0 = -60$ mV and $\zeta_p = -40$ mV, respectively, and the bulk ionic concentration is $n_0 = 1 \times 10^{-5}$ M.

observed. Similarly, for the second transition region negative ions are transported from the region above the heterogeneous patch to the homogeneous region, resulting in a decrease in the positive net charge density and an opposite disturbance of the local double layer field.

III.D. Influence on the Streaming Potential. As was discussed earlier, measurement of the streaming potential, whether dynamic or static, is a common method of characterizing the degree of surface heterogeneity. As was discussed by Norde and Rouwendal,[1] for flat surfaces the measured streaming potential should be linearly proportional to the area-averaged ζ-potential, ζ_{ave}, via the classical Smoluchowski equation given below,

$$\frac{\Delta E}{\Delta p} = \frac{\epsilon_w \zeta_{ave}}{\mu \lambda} \tag{6}$$

where λ is the total conductivity, E is the measured streaming potential, and p is the total pressure drop. To investigate this, a series of simulations were conducted using the loose-packed heterogeneous surface pattern (Figure 1B) with $L = 50\ \mu$m and $W = 25\ \mu$m with a heterogeneous patch ζ-potential of -20 mV in a 1×10^{-5} M KCl solution for various degrees of surface heterogeneous coverage. The total streaming potential across the periodic cell, ΔE, was calculated by integrating the result of eq 5c along the x-axis. The results are shown in Figure 13, where it can be seen that the model prediction matches quite closely this analytical result, thereby providing further validation of the numerical and analytical model. In general, this result was found to be consistent for the range of Reynolds numbers, ζ-potentials, and bulk ionic conductivities investigated here.

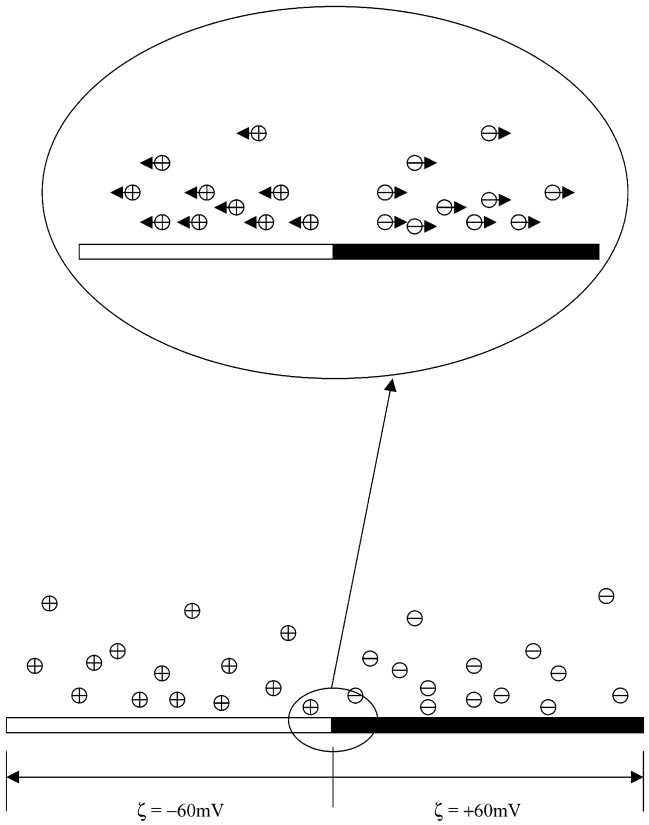

Figure 11. Diagram showing net charge density within the double layer region for the case of a homogeneous surface ζ-potential of -60 mV and an oppositely charged patch of $+60$ mV, where the flow is directed into the paper. The detailed image shows the applied body force on the local charges due to the induced electric potential gradient between the positive and negative surfaces.

As was shown in a previous paper,[30] the electroviscous effect tends to reduce the flow velocity in the double layer region resulting in an overall lower than expected streaming potential. To investigate the effect of channel height on the streaming potential, the loose-packed heterogeneous surface pattern, having 25% heterogeneous coverage, was used with the same dimensions, ζ-potential and ionic concentration, and Reynolds number as the case shown in Figure 3B for channel half-heights (l_y from Figure 2) varying from 5 to 25 μm. The results of these simulations are shown in Figure 14. As can be seen, the smaller channel sizes tend to show a slightly lower streaming potential and the result appears to be asymptotically approaching the analytical result as the channel size becomes larger, never differing by more than 5% of the analytical value.

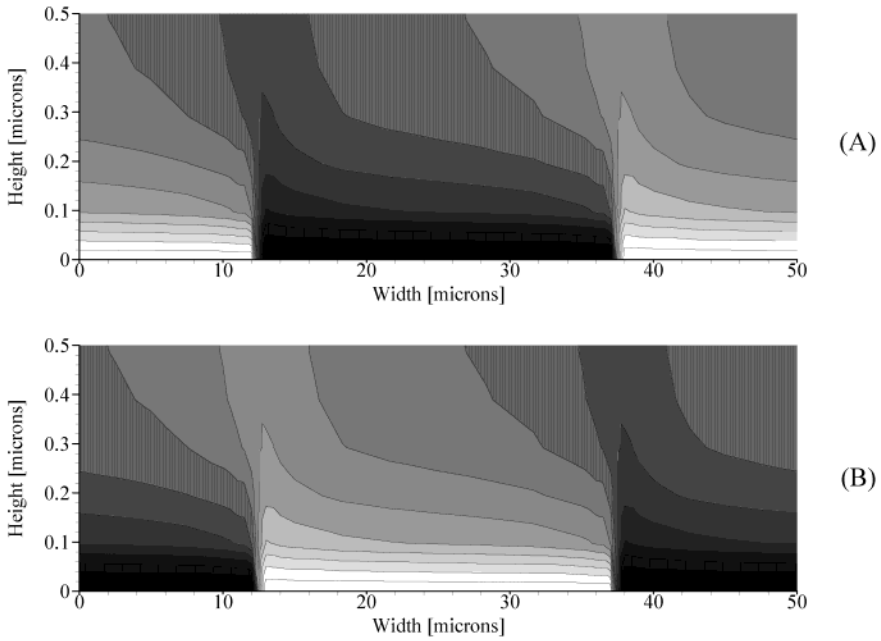

Figure 12. Electrostatic potential contours in the double layer region parallel with the flow axis on (A) Γ_5 ($z = 0$ μm) and (B) Γ_6 ($z = 25$ μm) surfaces with Re = 10.0 for the close-packed heterogeneous surface pattern. In each case, the ζ-potentials of the homogeneous region and heterogeneous patch are $\zeta_0 = -60$ mV and $\zeta_p = +60$ mV, respectively, and the bulk ionic concentration is $n_0 = 1 \times 10^{-5}$ M.

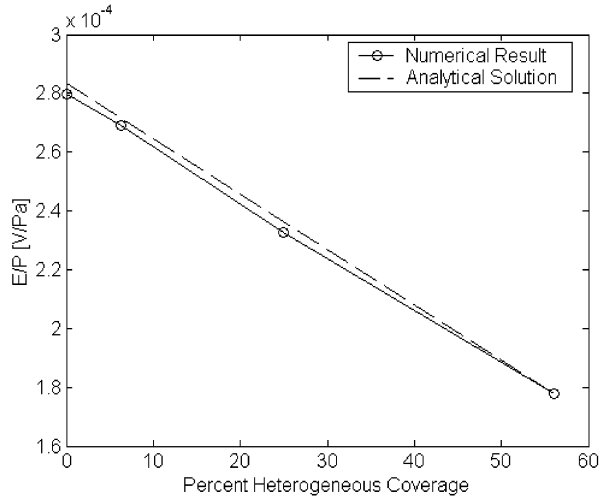

Figure 13. Influence of percentage heterogeneous coverage on the streaming potential for the loose-packed pattern. In all cases, Re = 1, the ζ-potentials of the homogeneous region and heterogeneous patch are $\zeta_0 = -60$ mV and $\zeta_p = -20$ mV, respectively, and the bulk ionic concentration is $n_0 = 1 \times 10^{-5}$ M. The analytical result is given by eq 6.

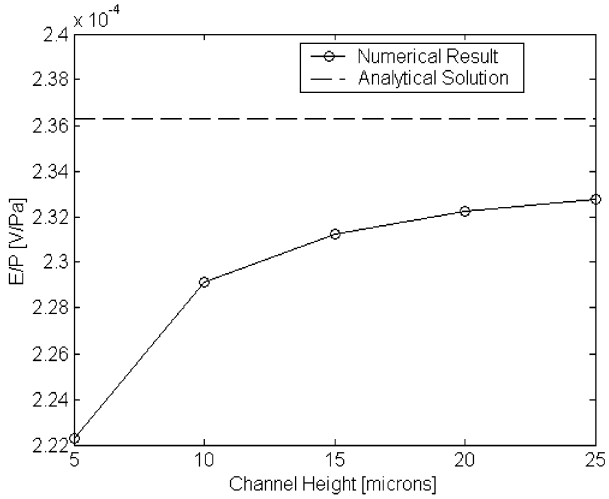

Figure 14. Influence of channel half-height on the streaming potential for the loose-packed pattern, and thus 25% heterogeneous coverage. In all cases, Re = 1, the ζ-potentials of the homogeneous region and heterogeneous patch are $\zeta_0 = -60$ mV and $\zeta_p = -20$ mV, respectively, and the bulk ionic concentration is $n_0 = 1 \times 10^{-5}$ M. The analytical result is given by eq 6.

IV. Summary and Conclusions

Surface electrokinetic heterogeneity occurs in a variety of electrokinetic characterization and microfluidic applications. In this study, a numerical model for pressure-driven flow over such surfaces, based on a simultaneous solution to the coupled Nernst−Planck, Poisson, and Navier−Stokes equations, was developed with the goal of investigating the resulting 3D flow structure and its effect on the electrical double layer distribution.

The presence of a heterogeneous patch was shown to induce a circulating flow pattern perpendicular to the main flow axis, which was caused by an electrostatic potential difference between the double layer field over the homogeneous surface and heterogeneous patch. Over the range investigated here, the strength of this circulation was found to be proportional to both Reynolds number and double layer thickness. At a higher Reynolds number (Re = 10), convective effects were found to be significant to the double layer distribution and led to a deviation from the classical Poisson−Boltzmann distribution observed at lower Reynolds numbers.

Acknowledgment. The authors are thankful for the financial support of the Natural Sciences and Engineering Research Council through a scholarship to David Erickson and through a research grant to D. Li. Additionally, the authors acknowledge Dr. Carsten Werner at the Institute for Polymer Research Dresden for his helpful discussions regarding the creation of heterogeneous surfaces.

LA025942R